Available online at www.sciencedirect.com
SCIENCE DIRECT®
PERGAMON
International Journal of Heat and Mass Transfer 46 (2003) 3451–3463
International Journal of HEAT and MASS TRANSFER
www.elsevier.com/locate/ijhmt

Condensation of bubbles in miscible liquids

H. Kalman *

Department of Mechanical Engineering, Pearlstone Center for Aeronautical Engineering Studies, Ben-Gurion University of the Negev, P.O. Box 653, Beer Sheva 84105, Israel

Received 11 December 2001; received in revised form 27 January 2003

Abstract

We previously developed a theoretical envelope model for bubbles condensing in immiscible liquids. The envelope model defines two zones while condensing. In the first zone the bubble accelerates after detachment from the nozzle and the heat is transferred through a viscous boundary layer at the front of the bubble and through the wake at the rear. In the second zone the bubble decelerates, settles into the wake and the heat is transferred through the wake all around the bubble. At a third zone, the bubble reaches the terminal velocity while the condensation process is terminated. In this paper both models (viscous boundary layer model—VBLM; and envelope model—EM) are modified to suit also bubbles condensing in miscible liquids. According to our visualization study of bubbles condensing in miscible liquids, partly envelopment of bubbles takes place at the deceleration zone. Visualization studies also revealed that the condensate mixes immediately with the surroundings. The experimental results for freon-113 bubbles condensing in subcooled freon-113 and presented in this paper confirm these observations and therefore they are bounded by two theoretical models: the envelope model and the viscous boundary layer model.

1. Introduction

Condensation of bubbles rising in cold liquid is a complicated problem to analyze. The condensation rate and the heat dissipation from the bubble are directly affected by three major parameters [1]: (1) The temperature difference of the condensing vapor and the surrounding liquid temperature, which is the driving force for the condensation heat transfer resulting from two thermal resistances; (2) the external thermal resistance due to the flow and heat transfer phenomenon in the condensing liquid near the bubble surface; and (3) the internal thermal resistance of the condensate that remains within the bubble (obviously for condensing in immiscible liquids). When the condensation rate is higher than the mixing rate of the noncondensible gases in the vapor, a third thermal resistance is added [2].

Experimental studies with bubbles condensing in miscible liquids have been previously conducted by Florschuetz and Chao [3] and Wittke and Chao [4]. These studies provide a very useful background for this research field, although the results could not be directly applied. Since then many papers have been published concerning bubble collapse in liquids, particularly about steam condensation in subcooled water. Kamei and Hirata [5] performed experimental analyses in which saturated steam bubbles, approximately 10 mm in diameter, were injected into quiescent subcooled water. The experiments were performed for pressure levels from atmospheric to 10^6 Pa and for temperature differences between the saturated steam and subcooled water ranging from 10 °C to 70 °C. Isikan [6] developed a theoretical equation to predict the collapse rate of spherical cap shaped bubbles. He determined the heat transfer both at the top surface and in the wake of the bubble. Chen and Mayinger [7] used holographic interferometry and high-speed cinematography to measure heat transfer at the phase interface of vapor bubbles condensing in a subcooled liquid of the same substance (ethanol, propanol, freon-113 and water). Zeitoun et al. [8] compared correlations for interfacial heat transfer between steam bubbles and subcooled water. They also

* Tel.: +972-8-6477099; fax: +972-8-6477101.
E-mail address: hkalman@bgumail.bgu.ac.il (H. Kalman).

0017-9310/03/$ - see front matter © 2003 Elsevier Science Ltd. All rights reserved.
doi:10.1016/S0017-9310(03)00128-5

Nomenclature

B	parameter (0 or 1) used in Eq. (17)
C_D	drag coefficient
CFF	condensation of R-113 in subcooled R-113
c_p	specific heat, J/kg °C
f	frequency of injection, bubbles/s
G	parameter for distinguishing between condensation in miscible and immiscible liquids, Eq. (1)
g	gravitational acceleration, m/s^2
H	position above the initial bubble, m
h	convection heat transfer coefficient, W/m^2 °C
h_{fg}	heat of vaporization, J/kg
k	thermal conductivity, W/m °C
m	mass, kg
Nu	Nusselt number $= (2Rh/k_L)$
Pr	Prandtl number $= (\mu c_p/k)_L$
q	rate of heat transfer, W
R	radius of bubble, m
Re	Reynolds number $= (2RU_\infty\rho_L/\mu_L)$
r	radius from the center of vapor sphere, m
T	temperature, °C
T_s	saturation temperature, °C
T_s^*	saturation temperature at partial vapor pressure, °C
T_∞	temperature of continuous liquid, °C
T_0	temperature of bubble surface, °C
t	time, s
U	potential velocity outside viscous boundary layer, m/s
U_∞	instantaneous rise velocity, m/s
u	velocity in the viscous boundary layer, m/s
y	distance (perpendicular) from bubble surface, m
Z	dimensionless quantity $\delta^2 U_\infty/\nu R$

Greek symbols

α	fraction of noncondensibles
γ	as defined by Eq. (13)
δ	thickness of viscous boundary layer, m
δ_f	thickness of condensate film, m
δ_t	thickness of thermal boundary layer, m
ΔT	temperature difference $= (T_s - T_\infty)$, °C
θ	angle from front stagnation point of vapor sphere
μ	viscosity, kg/ms
ρ	density, kg/m^3
ϕ_s	normalized saturation temperature, Eq. (7)
ξ	ratio of boundary layer thickness (thermal to viscous)

Subscripts and superscripts

b	bubble
f	condensate
L	continuous liquid
0	initial or front stagnation point
r	rear
v	vapor
$^-$	non-dimensional length, dividing by R_0

carried out experiments from which they obtained a new correlation for bubble condensation Nusselt number in a multi-bubble system. However, all the above models concerned pure systems without the presence of noncondensibles, and assumed constant rising velocities.

Theoretical and experimental studies on condensing, steadily rising, hydrocarbon bubbles in water were conducted by Jacobs [2,9] and Sideman [10,11]. Both these investigators assigned a thermal boundary layer to the bubble. In Sideman's model viscous effects were semi-empirically accounted for by a "velocity factor". Jacobs assumed a potential flow field around the bubble, and introduced the condensate film inside the bubble as a substantial thermal resistance factor. In Sideman's model the condensate film was assumed to be negligible.

Higeta et al. [12,13] conducted an extensive experimental research study of condensation in immiscible liquids from which they defined three patterns of condensation, all of which are dependent on how the condensate 'wets' the coolant surface. To gain insight into the physical phenomena governing bubble collapse in immiscible liquids, visualization studies were conducted by Kalman et al. [14,15]. The temperature field was visualized by shadowgraphing and the flow field by color entrainment. The bubble shape and trajectory were videotaped and screen-traced, and the condensate shape inside the bubble was visualized by dye injection.

All these studies together present a clear picture of the physical phenomena governing the process of bubbles condensation. The vapor appears as a sphere eccentrically positioned in the bubble at its top. The condensate film seems to adhere to the bubble surface, grow in thickness from the nozzle, and then the collapsing bubble accelerates. A viscous boundary layer extends over the upper surface of the bubble and a wake over its rear surface. As the bubble reaches its maximum velocity, it begins to decelerate, settling into its wake. An "envelope" of vortices surrounds the bubble until collapse is concluded. These phenomena were observed in freon-113—water system, as well as in various hydrocarbons—

water systems. The visualization led to the development of the "envelope model" for intermediate size bubbles [14,16,17]. The model is expressed by the collapse rate equation and the appropriate velocity expression. The envelope model conforms to good wettability patterns according to Higeta et al.'s [12,13] analysis.

In this paper, the envelope model is developed further and generalized to include condensation in miscible liquids. By the generalized equations both systems of condensation can be solved. The theoretical model can be applied to obtain an accurate solution although some simple correlations were published previously by Kalman and Mori [1].

2. Experimental apparatus

The condensation experiments and the visualization study were conducted with freon-113 bubbles in subcooled freon-113. The process took place with the same experimental apparatus used in condensation experiments for immiscible liquids [16] with some slight adjustments, as follows. The bubble collapse was conducted in a vertical square column, 10×10 cm in cross section, and 60 cm high, as shown in Fig. 1. The walls of the column were made of glass plates. Beneath the glass column a vapor generator made of a brass cylinder was installed. It was filled with water, electrically heated, and thermostatically controlled. A copper tube passed through the vapor generator to the bottom of the glass column and into the injection nozzle. The glass column was filled with freon-113 at a prescribed temperature, and was open to the atmosphere. The prescribed temperature of the surrounding freon-113 was achieved by circulation through an external thermostatically controlled container filled with water.

3. Visualization study

An extensive visualization study of freon-113 bubbles condensing in water has been performed previously by Kalman et al. [15]. The study comprised the following procedures: screen tracing, visualization of the condensate shape, visualization of the temperature field outside the bubble by shadowgraphing and visualization of the flow field around the bubble. The visualization study resulted in three major findings (assumptions) that were used to develop the envelope model [16]:

1. The bubble is spherical during the collapse process (at least at the final stages of collapse).

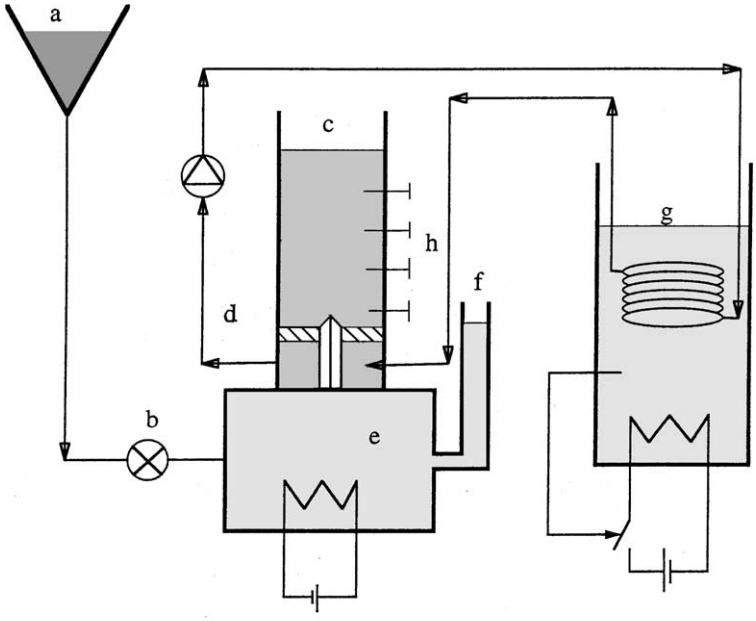

Fig. 1. Schematic diagram of the experimental setup.

2. The condensate remains with the bubble to form a two-phase bubble. The vapor bubble is spherical and adheres to the top of the two-phase bubble.
3. The bubble detached from the nozzle first accelerates and then decelerates. At the acceleration zone the bubble has a viscous boundary layer at the front and a wake at the rear. However, at the deceleration zone the bubble sinks into its wake and is enveloped by it.

In the visualization study that follows we will attempt to compare the behavior of particles condensing in miscible liquids to bubble collapse in immiscible liquids. The applicability of the above three findings for condensation in miscible liquids will also be examined.

3.1. Screen tracing

Fig. 2 shows screen tracing of a freon-113 bubble condensing in water (Fig. 2a) and a freon-113 bubble condensing in subcooled freon-113 (Fig. 2b). The detachment of the bubble results in a strong deformation that is followed by a series of shape oscillations in which the bubble oscillates between oblate and prolate shapes. As the collapse process in immiscible liquid proceeds, the bubble gradually becomes spherical as a result of the decrease in its radius of curvature and the consequent increase of surface-tension forces. In comparison, for condensation in miscible liquids, the bubble remains oblate due to the low surface tension of the organic bubble [18].

3.2. Condensate shape

The condensate shape of bubbles condensing in immiscible liquids is of great importance for defining internal thermal resistance. The condensate shape was visualized in two ways: by casting a shadow of the vapor bubble and by coloring the liquid condensate. Fig. 3 shows four Hexane bubbles condensing in water at different stages of collapse. In these photographs the vapor appears black, and the external interface between the condensate and the water is distinctly outlined. The images show the two-phase bubble shape at different stages of collapse. Bottom image presents a bubble at the early stages of collapse when the condensate is a thin layer appearing mainly at the bottom of the bubble. Then the condensate volume increases and a two-phase bubble, which contains a vapor bubble adhering to the two-phase bubble at the top, is established. The condensate film cannot be seen at the top of the bubbles, perhaps because the black vapor bubble has concealed the thin condensate film that could have been maintained at the upper part of the bubble. Nevertheless, this figure confirms the finding of Kalman et al. [15] for

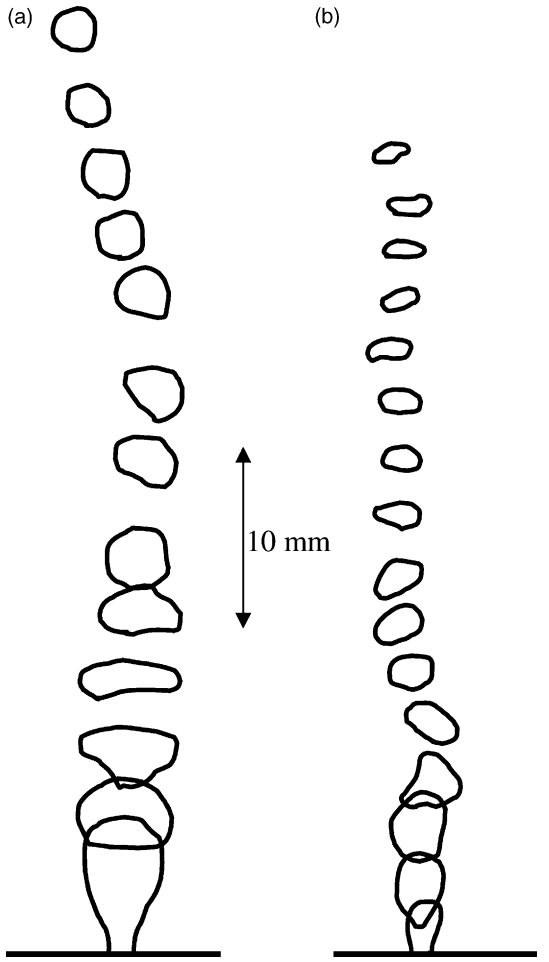

Fig. 2. Screen tracing of a bubble of freon-113 (a) condensing in water, (b) condensing in subcooled freon-113.

freon-113 bubbles condensing in water and therefore may be extended for any bubble condensing in immiscible liquids.

The condensate shape for condensation in miscible liquids is obviously not the same as for condensation in immiscible liquids. The important question we must ask concerns the intensity of the condensate mixing with the surroundings, which can only be solved by experimental and visualization studies. If the condensate remains with the collapsing bubble for a while, it could maintain a thermal resistance similar to the thermal resistance for the immiscible case.

Since it is impossible to cast a shadow of the mixing condensate in the miscible case, we use the following alternative method. In this case a colored droplet should evaporate (this is in order to keep the dye in the bubble) to form a bubble and then condensate. This method was performed in a square column that was divided into three parts by two insulating plates, as shown in Fig. 4.

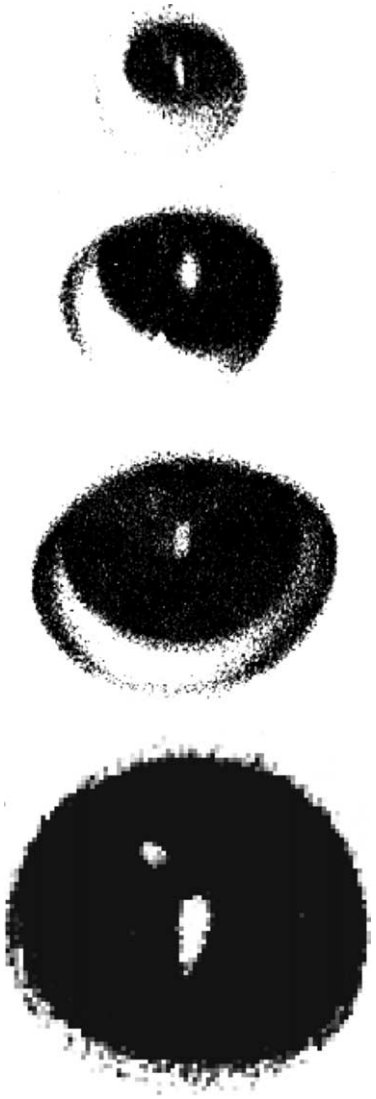

Fig. 3. Condensate shape of hexane bubbles condensing in water at different stages of collapse.

The lower part consisted of cold water, the central part consisted of hot water, and the upper part consisted of water at the condensation temperature where a glass tube contains the miscible condensing liquid. To implement such an arrangement requires that we test a hydrocarbon that has a lower density than the water. According to this arrangement a colored pentane droplet can be injected at the lower part, rise to the middle part for evaporation, and continue to the glass tube for condensation.

The bubbles that reached the water–pentane interface were delayed for a while due to interfacial forces and surface tension. This was followed by one of two situations: either the bubble moved up and was enveloped

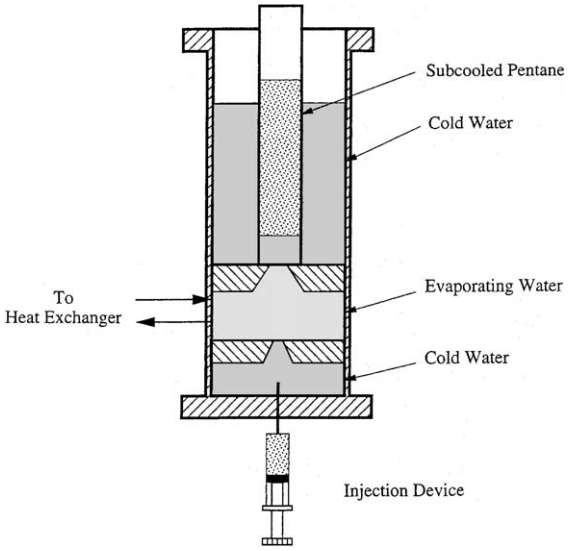

Fig. 4. The experimental column for visualizing the mixing process of the condensate while condensing in miscible liquids.

by the water to maintain a three-phase bubble (i.e., pentane vapor with pentane condensate inside the water envelope), or the bubble collapsed in the subcooled liquid. In the first situation, in most cases the three-phase bubble reached the upper pentane–air interface for phase separation. In some cases, the water envelope was removed during the collapse by shear forces, and immediate mixing of the colored condensate in the surrounding liquid occurred. In the second situation, the bubble entered the pentane tube without the water envelope, and quick mixing of the condensate took place (see Fig. 5).

3.3. Flow field outside the bubble

Flow and temperature fields outside the bubble play an important part in defining the external thermal resistance. The temperature field outside a freon-113 bubble condensing in water has been previously visualized by shadowgraphing [16,19]. The shadowgraphs of freon-113 bubbles condensing in water revealed three zones of interest during collapse. As the bubble gets detached from the nozzle, the bubble accelerates and a thermal wake is formed at the rear and a thermal boundary layer at the front. In the second zone, the bubble decelerates due to decreasing dimensions and increasing average density. In the deceleration zone, the thermal cloud of the wake moves towards the bubble and envelops it. In the third zone, while the condensation process is terminated, the bubble moves at the terminal velocity. At this stage the wake detaches from the bubble.

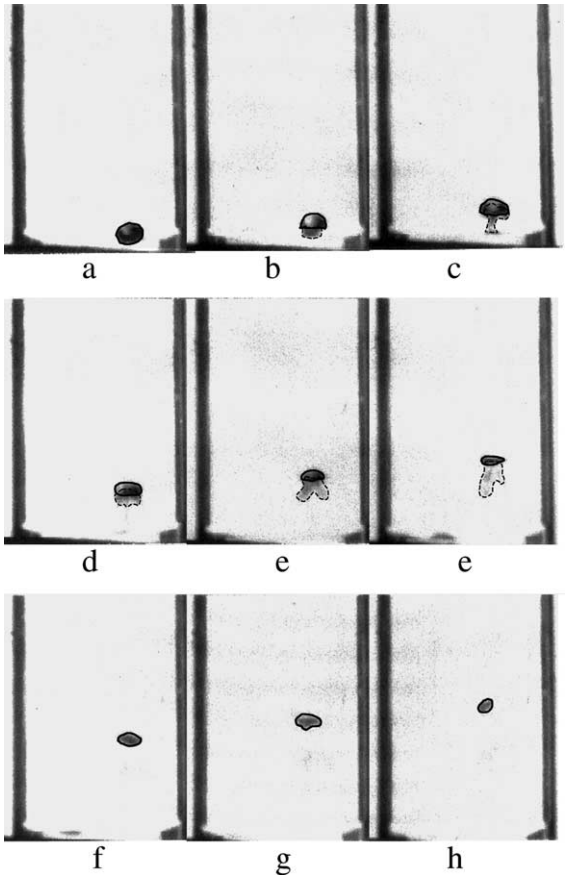

Fig. 5. Visualization of the mixing process of the condensate of a pentane bubble condensing in subcooled pentane.

The flow field and viscous effects were visualized by injecting the bubble into the test section through a layer of colored water (by $KMnO_4$) above the nozzle [15]. The viscous effects confirmed the same behavior that was detected for the thermal field. Another series of freon-113 bubble condensing in water is shown in Fig. 6. Photographs (a–c) illustrate a bubble at the first zone; photographs (d–e) show the bubble at the second zone; and the third zone appears in photographs (g, h). To elucidate if this phenomenon is valid only for freon-113 bubbles (that their liquid density is higher than the water density), a similar visualization for pentane bubble condensing in water is presented in Fig. 7.

The same technique was applied for condensation in miscible liquids using an organic dye instead of $KMnO_4$. Fig. 8 illustrates a bubble of freon-113 condensing in subcooled freon-113. In this figure, a thin tube through which the organic dye was injected into the nozzle can be seen at the left side. Even though the wake appears to be light, the envelopment, or at least a partial envelopment, can be observed in photographs (c–e).

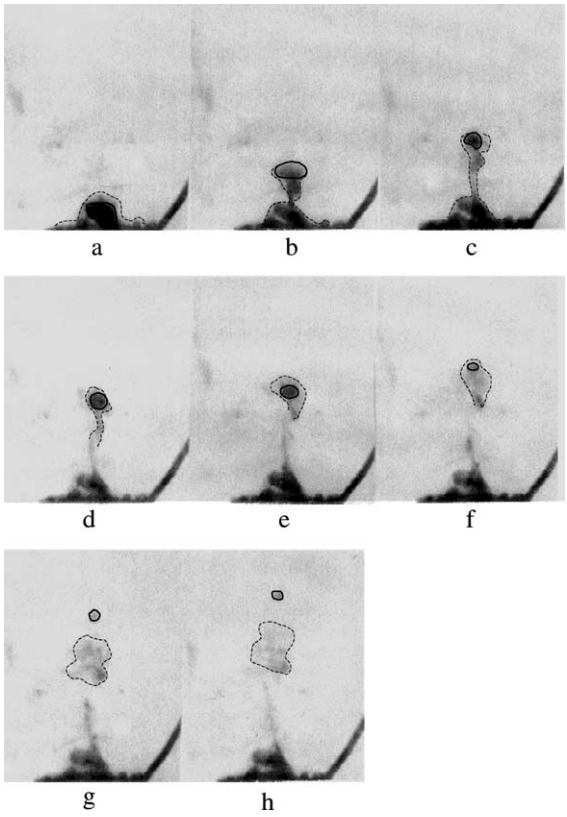

Fig. 6. Flow field and envelopment of a freon-113 bubble condensing in water.

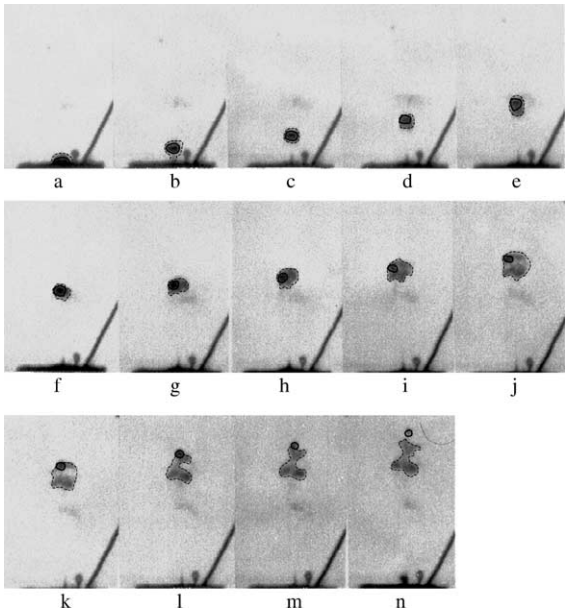

Fig. 7. Flow field and envelopment of a pentane bubble condensing in water.

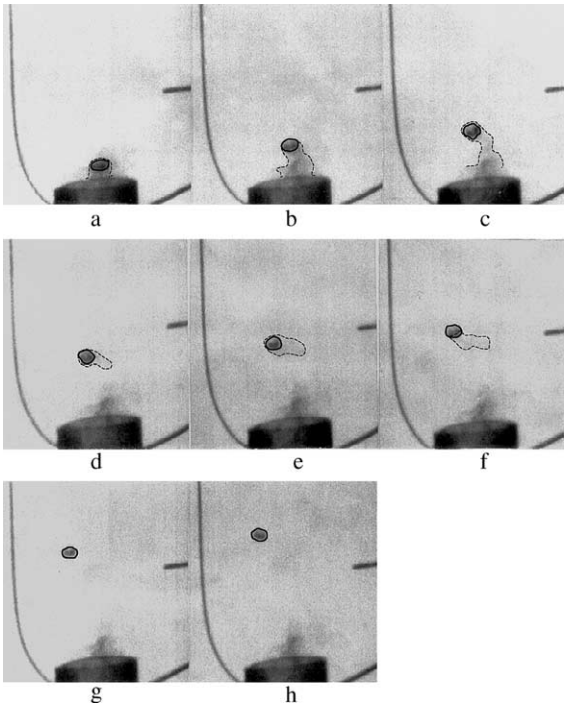

Fig. 8. Flow field and partial envelopment of a freon-113 bubble condensing in subcooled freon-113.

4. The theoretical model

The visualization study of bubble condensation in miscible liquids demonstrates the same phenomenon of envelopment as bubbles condensing in immiscible liquids, although less clearly. Therefore, it is feasible that a theoretical model similar to that developed previously for condensation in immiscible liquids [16] can be developed. The visualization study also confirmed that immediate mixing of the condensate with the surroundings takes place. On this premise, we redeveloped the previous model in a general form such that it would be suitable for condensation of bubbles in either miscible or immiscible liquids. The model is based on the following assumptions that are applicable for condensation in immiscible [16] or miscible liquids and shown schematically in Fig. 9:

1. The bubble is spherical. An equivalent radius is used in zones where shape oscillations and distortion take place.
2. In the case of condensation in immiscible liquids, the sphere of vapor is eccentrically positioned in the top of the bubble. The condensate film adheres to the surface of the bubble. It does not flow or drain. It grows in thickness as the collapse proceeds.
3. The initial bubble consists of saturated vapor and noncondensible gases. The noncondensibles are uniformly distributed in the vapor.
4. The bubble velocity is translational and time dependent. The drag coefficient may vary as a function of size and shape.
5. The liquid surrounding the bubble is quiescent, infinite, and has a constant temperature.
6. A viscous liquid surrounds the bubble. A nonslip condition is assumed at the bubble surface. The flow field is potential outside the viscous boundary layer.

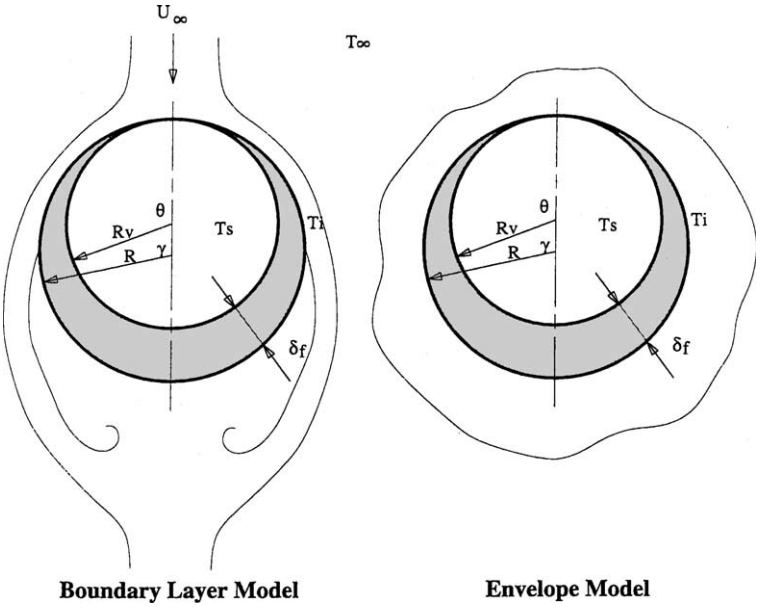

Fig. 9. A schematic diagram of the two-phase bubble and the nomenclature related to the bubble geometrical dimensions.

7. A thermal boundary layer extends from the bubble surface into the viscous layer. The temperature field outside the thermal boundary layer is quasi-steady, i.e., it instantaneously adjusts to the shape and size of the collapsing bubble.
8. In the acceleration zone, a viscous boundary layer extends over the upper surface of the bubble, and a wake appears over the rear surface. In the deceleration zone the bubble settles into its wake (though not fully in cases of condensation in miscible liquids). An "envelope" of vortices concentrically surrounds the bubble. The flow field outside the "envelope" is preserved.

We use Isenberg et al.'s [10] parameter 1/G for distinguishing between the two systems, as follows:

$$\frac{1}{G}=\frac{\rho_v}{\rho_f} \quad \text{immiscible}$$

and

$$\frac{1}{G}=0 \quad \text{miscible} \tag{1}$$

For bubbles condensing in immiscible liquids, the rate of heat transferred from the bubble to the surroundings was obtained previously [16]. The nomenclature is presented in Fig. 9.

$$q=\int_0^{\pi}\frac{\pi R_0(T_s^*-T_\infty)\sin\theta\,d\theta}{\frac{1}{2k_f}\left[\frac{1}{\overline{R}_v}-\frac{1}{\overline{R}_v+\bar{\delta}_f}\right]+\frac{\overline{R}}{Nuk_L(\overline{R}_v+\bar{\delta}_f)^2}} \tag{2}$$

where $\bar{\delta}_f=\delta_f/R_0$ and $\overline{R}_v=R_v/R_0$.

The two terms of the denominator relate to the thermal resistances in line. The first relates to the conductive thermal resistance of the condensate film—the internal resistance. The second relates to the convective thermal resistance of the surrounding—the external resistance. By combining Eq. (2) with the heat of condensation equation we get

$$\frac{d\overline{R}}{dt}=-\frac{q}{4\pi\overline{R}^2R_0^3\rho_v h_{fg}} \tag{3}$$

Then, the rate of bubble collapse is obtained from Eq. (3) as:

$$\frac{d\overline{R}}{dt}=-\frac{(T_s^*-T_\infty)}{4R_0^2\rho_v h_{fg}\overline{R}^2}\int_0^{\pi}\frac{\sin\theta\,d\theta}{\frac{1}{2k_f}\left[\frac{1}{\overline{R}_v}-\frac{1}{\overline{R}_v+\bar{\delta}_f}\right]+\frac{\overline{R}}{Nuk_L\left(\overline{R}_v+\bar{\delta}_f\right)^2}} \tag{4}$$

Based on a mass balance for the case of condensation in miscible liquids $\frac{4}{3}\pi R_0^3\rho_v=\frac{4}{3}\pi R_v^3\rho_v+\frac{4}{3}\pi(R^3-R_v^3)\rho_f$, we may write for $\overline{R}_v$:

$$\overline{R}_v=\left[\frac{\overline{R}^3-\frac{1}{G}}{1-\frac{1}{G}}\right]^{1/3} \tag{5}$$

For condensation in miscible liquids, we insert $1/G=0$ into Eq. (5) which results in $\overline{R}_v=\overline{R}$ according to the assumption that no condensate is maintained in the collapsing bubble. Therefore, the vapor radius is equal to the total collapsing bubble radius. In the case of condensation in immiscible liquids, the bubble radius is larger than the vapor radius due to the presence of the condensate.

We can define $\bar{\delta}_f$, by geometric considerations:

$$\bar{\delta}_f=\left[\overline{R}_v(2\overline{R}-\overline{R}_v)+(\overline{R}-\overline{R}_v)^2(\cos\theta)^2\right]^{1/2}-(\overline{R}-\overline{R}_v)\cos\theta-\overline{R}_v \tag{6}$$

For condensation in miscible liquids, we substitute $\overline{R}_v=\overline{R}$ into Eq. (6), which results in $\bar{\delta}_f=0$ according to the assumption that no condensate is maintained in the collapsing bubble.

The apparent temperature driving force $(T_s^*-T_\infty)$ has been studied comprehensively by Ullmann and Letan [20] and has been applied in the dimensionless form [2,11,21] as:

$$\phi_s=\frac{T_s^*-T_\infty}{T_s-T_\infty}=\frac{\overline{R}^3-\overline{R}_f^3}{\overline{R}^3-\frac{1}{G}} \tag{7}$$

For the general case, inserting $(T_s^*-T_\infty)$ from Eq. (7) into Eq. (4), yields:

$$\frac{d\overline{R}}{dt}=-\frac{(T_s^*-T_\infty)}{4\rho_v h_{fg}}\left[\frac{\overline{R}^3-\overline{R}_f^3}{\overline{R}^3-\frac{1}{G}}\right]\frac{1}{R_0^2\overline{R}^2}\times\int_0^{\pi}\frac{\sin\theta\,d\theta}{\frac{1}{2k_f}\left[\frac{1}{\overline{R}_v}-\frac{1}{\overline{R}_v+\bar{\delta}_f}\right]+\frac{\overline{R}}{Nuk_L(\overline{R}_v+\bar{\delta}_f)^2}} \tag{8}$$

For condensation in miscible liquids Eq. (8) can be simplified by inserting $\frac{1}{G}=0$, $\overline{R}_v=\overline{R}$ and $\bar{\delta}_f=0$.

$$\frac{d\overline{R}}{dt}=-\frac{(T_s^*-T_\infty)k_L}{4R_0^2\rho_v h_{fg}\overline{R}}\left[1-\left(\frac{\overline{R}_f}{\overline{R}}\right)^3\right]\int_0^{\pi}Nu\sin\theta\,d\theta \tag{9}$$

The thermal resistance outside the bubble, namely the convection heat transfer over the bubble surface, expressed by the heat transfer coefficient, h, appears in the definition of Nu in Eqs. (8) and (9). The solution of Lee and Barrow [22] has been applied in the Nusselt number over the upper surface of an accelerating bubble:

$$Nu=2.83\frac{Re^{1/2}}{\xi Z^{1/2}} \tag{10}$$

Approximations of Z [23] and $\xi=\xi_{\theta=0}=\xi_0$ [24] were introduced into Eq. (10) to yield:

$$Nu = \frac{0.594}{\xi_0} \frac{\sin^4 \gamma Re^{1/2}}{\left[\int_0^\theta \sin^7 \gamma \, d\gamma\right]^{1/2}} \tag{11}$$

within $0 \leqslant \gamma \leqslant \frac{\pi}{2}$ in the acceleration zone.

For the heat transfer coefficient at the rear half of the bubble the empirical relation of Lee and Barrow [22] is used:

$$Nu_r = 0.0447 Re^{0.78} Pr^{1/3} \tag{12}$$

over the range of $\frac{\pi}{2} < \gamma \leqslant \pi$ in the acceleration zone.

In the deceleration zone, Eq. (12) is used all over the bubble surface, within $0 \leqslant \gamma \leqslant \pi$, according to the envelope model.

To determine the Nusselt number, the angle γ is used instead of θ because of the eccentricity of the vapor in the bubble. The definitions of both angles are shown in Fig. 9 and are related by:

$$\gamma = \sin^{-1}\left[\frac{\overline{R}_v + \bar{\delta}_f}{\overline{R}} \sin\theta\right] \tag{13}$$

Note that $\gamma = \theta$ for condensation in miscible liquids when $\overline{R}_v = \overline{R}$ and $\bar{\delta}_f = 0$.

To use the Nusselt number of Eq. (11), the boundary layer ratio at the front stagnation point, ξ_0, has to be applied. Kalman and Letan [24] showed that the boundary layer ratio remains constant over the front half of a mobile surface bubble, at least up to about 70° from the front stagnation point.

Extension of ξ_0 up to the equator is a reasonable approximation, since the heat flux is maximum at the front stagnation point and decreases towards the equator [24]. Kalman and Letan's work extended to Lee and Barrow's [22] solid sphere model by taking into account a mobile surface. The boundary layer ratio at the front stagnation point, ξ_0, applied to Eq. (11) as a function of the Prandtl number is based on Kalman and Letan's model (see the Appendix A). The mobility parameter n indicates the ratio between the surface and the external velocities in the following way:

$$u_{y=0} = \frac{1}{n} U \tag{14}$$

where $1 \leqslant n \leqslant \infty$. $n = 1$ represents a mobile surface at the external velocity (without a viscous boundary layer) and $n = \infty$ represents a rigid surface.

In our previous works concerning condensation in immiscible liquids, an immobile bubble surface was assumed. This was reasonable since impurities are present in the liquids and also because the thin condensate film adheres to the bubble surface. The condensate film itself could act as an impurity that would increase the surface tension and reduce the surface mobility. However, in the case of condensation in miscible liquids, the condensate film is mixed into the surroundings and the bubble may perform some degree of surface mobility, as will be discussed later.

The collapse rate equation (8) or (9) of the bubble has to be accompanied by the appropriate bubble velocity equation. In zones of time-dependent bubble mass (miscible condensate), the instantaneous velocity is based on a momentum balance:

$$\frac{d(mU_\infty)}{dt} = \frac{4}{3}\pi R^3 g(\rho_L - \rho_b) - \pi R^2 C_D \frac{\rho_L U_\infty |U_\infty|}{2} \tag{15}$$

where ρ_b is the bubble's average density. If the added mass from the surroundings has a half volume of the bubble, the total mass is:

$$m = \left(\rho_b + \frac{1}{2}\rho_L\right)\frac{4}{3}\pi R^3 \tag{16}$$

Inserting Eq. (16) into Eq. (15) and differentiating the momentum term yields a first order nonlinear differential equation:

$$\frac{dU_\infty}{dt} = \frac{8\overline{R}R_0 g(\rho_L - \rho_b) - 3C_D\rho_L U_\infty|U_\infty| - 24B\left(\rho_b + \frac{1}{2}\rho_L\right)U_\infty R_0 \frac{d\overline{R}}{dt}}{8\left(\rho_b + \frac{1}{2}\rho_L\right)\overline{R}R_0} \tag{17}$$

which is suitable for condensation in either miscible or immiscible liquids by inserting the appropriate values of B and ρ_b.

For condensation in miscible liquids:

$$B = 1 \quad \text{and} \quad \rho_b = \rho_v \tag{18}$$

and for condensation in immiscible liquids:

$$B = 0 \quad \text{and} \quad \rho_b = \frac{\rho_v}{\overline{R}^3} \tag{19}$$

The drag coefficient C_D of a rigid sphere is [1,16]:

$$C_D = \frac{16}{Re} + \frac{6}{1 + Re^{1/2}} + 0.4 \tag{20}$$

The drag coefficient of a spheroid can be applied to Eq. (17) as well.

The simultaneous solution of Eqs. (8) and (17) yields the instantaneous radius, $\overline{R}(t)$, and velocity $U_\infty(t)$, which can be integrated with respect to time to yield the path (height above nozzle) of the bubble.

$$H = \int_0^t U_\infty(t)\, dt \tag{21}$$

The solution involves parameters that can be independently varied. These include the initial radius of the

injected bubble, R_0, the temperature driving force, ΔT, and the fraction of the noncondensibles, α, as expressed by the final radius, $\overline{R}_f$.

5. Results and discussion

The extensive visualization studies of freon-113 bubbles condensing in water performed in previous works included shadowgraphing, color entrainment in wakes, visualization of condensate, and screen tracing [15,16]. These studies have been further applied to pentane and hexane bubbles condensing in water [14]. In this paper, we performed visualization studies of bubbles condensing in miscible liquids. The experiments clearly showed that the condensate mixes immediately into the surroundings for condensation in miscible liquids. At the same time, envelopment of bubbles by their wake appears to exist only partly and for shorter times compared to condensation in immiscible liquids. However, part envelopment is not included in the theoretical envelope model presented in this paper and is difficult to define. Therefore, the experimental measurements, shown in Figs. 10–14, were compared to theoretical analysis by plotting two theoretical lines for some of the cases. One theoretical line is ascribed to the model of envelopment and the other to the viscous and thermal boundary layers at the front half of the bubble during the entire collapse process. The main difference between the models can be defined by the equation used for the heat transfer coefficient. For the viscous boundary layer (VBL) model and for the acceleration zone of the envelope model we used Eq. (11) for the front half and Eq. (12) for the rear half of the bubble during all stages, and for the deceleration zone of the envelope model we used Eq. (12) only. These models function as borderlines for the experimental results.

In most cases, the experimental results, for higher temperature differences, appeared in-between the two theoretical borderlines (Figs. 10–12). In some cases, they

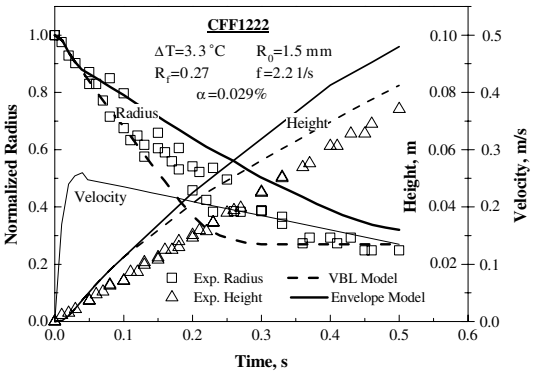

Fig. 10. Condensation of freon-113 bubbles in subcooled freon-113: comparison of the model with experiment no. CFF1222.

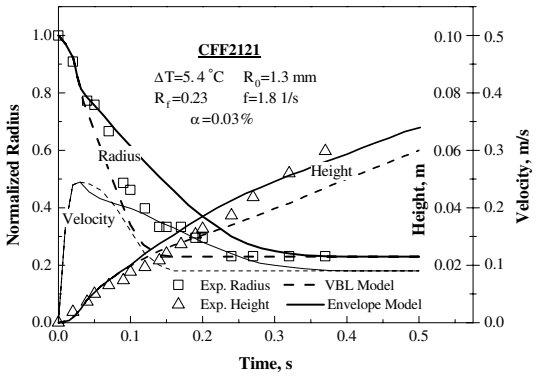

Fig. 11. Condensation of freon-113 bubbles in subcooled freon-113: comparison of the model with experiment no. CFF2121.

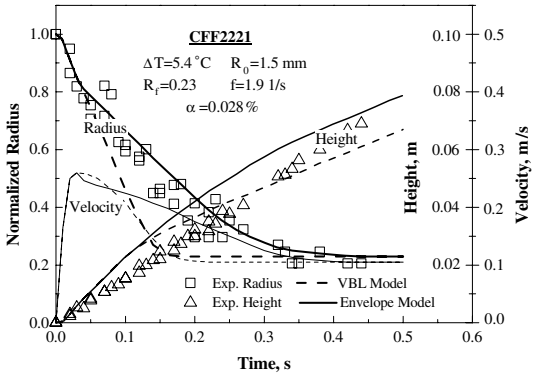

Fig. 12. Condensation of freon-113 bubbles in subcooled freon-113: comparison of the model with experiment no. CFF2221.

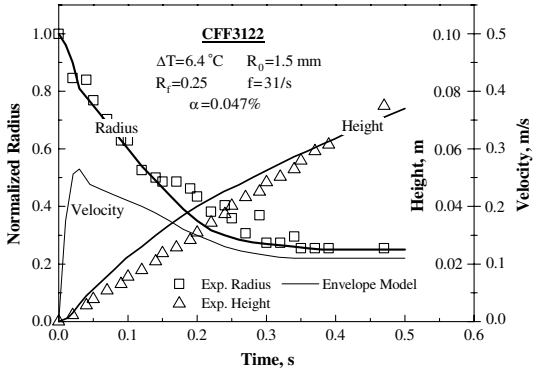

Fig. 13. Condensation of freon-113 bubbles in subcooled freon-113: comparison of the model with experiment no. CFF3122.

appeared slightly above the upper limit (Figs. 13 and 14). The lower condensate rate in some of the experimental results could be due to the assumption that the bubbles are spherical. By looking again at the screen tracing (Fig. 2) we confirm that assuming that the

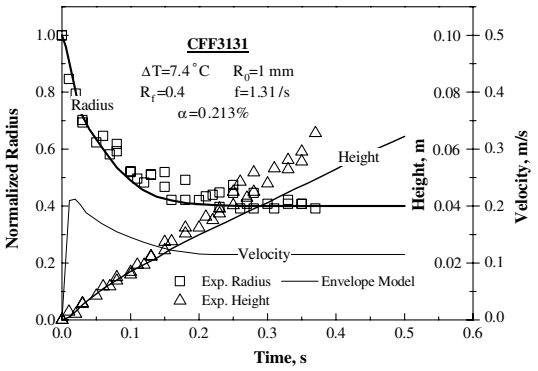

Fig. 14. Condensation of freon-113 bubbles in subcooled freon-113: comparison of the model with experiment no. CFF3131.

bubbles are spherical for condensing in miscible liquids might be inaccurate. The bubbles are shaped more like spheroids. Another reason for low condensation rate could be the effect of the condensate. The condensate was assumed to mix immediately into the surroundings without affecting either the heat transfer or the flow outside the bubble. Since the mixing process takes some certain amount of time, even if it is short, the condensate first flows downward at the bubble surface. This could be a reason to increase the boundary layer and consequently reduce the heat transfer rate from the bubble to the surroundings.

In one of the experiments, the experimental heights are lower than the theoretical predictions (Fig. 10) and only in one case did the theoretical model under-predict the experimental heights (Fig. 14). There are two reasons for providing higher velocities in the theoretical model. The first concerns the assumption that the bubble is spherical for which reason a drag coefficient, C_D, of a sphere was applied. However, inserting a drag coefficient of a spheroid would reduce the velocity, though not enough to conform to the theoretical model. Also it could have a very little effect on the theoretical collapse lines. The second reason is related to the rising bubble mass. It was assumed that the accelerating bubble contains the instantaneous vapor mass and the added mass (the surrounding liquid whose volume is half that of the vapor bubble). Since the condensate initially maintains the bubble velocity and acceleration, at least part of it should be contained in the bubble mass.

The experiments presented in this work (Figs. 10–14) were conducted at low injection frequencies of 1.3–3 bubbles/s. The injection frequency of $f \leqslant 3$ bubbles/s is far below the frequency of interaction. Hence, the injection frequency does not serve as a parameter in that range. The initial radii were $1–1.5 \times 10^{-3}$ m. The temperature difference ranged between 3.3 and 7.4 °C, and the fractions of noncondensibles corresponded to 0.028–0.213%.

The initial radii shown in Figs. 10–14 are smaller than those we experienced for condensation in immiscible liquids, although the same nozzles were used. The largest bubble had an initial radius of 1.5 mm while for condensation in immiscible liquids initial radii of up to 2.6 mm were detected. This is a result of the higher buoyancy forces while condensing in freon-113 (about 1.5 times) than the cases of condensing in water (due to the higher density). The small radii are also due to lower surface tension forces between freon-113 vapor and liquid freon-113 than between freon-113 vapor and water. The surface tension plays a major role in the detachment process at the necking for low injection frequencies.

During condensation, the final radii are also smaller for miscible liquids than for immiscible liquids. Theoretically, the bubble could be condensed entirely in pure systems without the presence of noncondensibles. In that case a bubble condensing in miscible liquid will disappear while a bubble condensing in immiscible liquid will collapse to a pure droplet.

The temperature difference of 3.3–7.4 °C appears to be satisfactorily expressed in the theoretical model. In our present experimental range, the Jacob number is smaller than 10, and the heat transfer rates control the collapse process. At much larger temperature differences, other unaccounted for effects in the present formulations may become dominant.

The fraction of noncondensibles in the bubble controls the apparent saturation temperature T_s^* in the bubble. This way the presence of noncondensibles reduces the temperature driving force that affects the rate of collapse, the size of the bubble, and the termination of the process. The fraction of noncondensibles presently experimented with was below 0.25%. These concentrations are very low and presumably do not affect the thermal resistance inside the bubble. At much higher concentrations, the thermal resistance may become affected. This will have to be accounted for in future research.

The main difference between condensation in miscible liquids and condensation in immiscible liquids is that in some cases envelopment only partly appears. In other cases, when the collapse rate is high and the deceleration is pronounced, the condensation characteristics are similar and the bubble is fully enveloped. However, even for the partly envelopment model exhibits an upper limit. The collapse rate is affected mainly by the temperature difference and initial radius.

6. Conclusions

A theoretical model for condensation of bubbles in miscible liquids was developed by considering an accelerating-decelerating bubble that shows two distinct zones of collapse. This model was based on our previous

envelope model for condensation in immiscible liquids. In acceleration the rate of collapse is steep. In deceleration, the bubble sometimes settles into its wake and then the rate of collapse abruptly decreases. In miscible liquids the condensate is assumed to mix immediately in the surroundings.

Since a bubble condensing in miscible liquid is partly enveloped and the ratio of envelopment cannot be defined quantitatively, two theoretical limit models were developed, namely the envelope model and the viscous boundary layer model. The envelope model provided the upper limits of the collapse rate and the boundary layer model, the lower limits. The experimental results confirmed the theoretical expectations—they were bounded by the theoretical limits. The discrepancy between theoretical and experimental paths of bubbles during collapse was shown to be related to the effect of the mixing condensate on the viscous boundary layer and the irregularity of the bubble shape.

Appendix A

Tomotika [25] and Lee and Barrow's [22] models were further extrapolated for mobile surface spheres by introducing the mobility parameter n (Eq. (14)). This yields a differential equation for the viscous boundary layer [22] for potential flow outside the boundary layer:

$$\frac{\mathrm{d}Z}{\mathrm{d}\gamma}=\frac{2}{3}K(\lambda)\frac{1}{\sin\gamma}-\frac{3}{2}H(\lambda)\sin\gamma Z^2-\frac{2}{3}K^*(\lambda)\frac{1}{\sin\gamma} \tag{A.1}$$

where

$$K(\lambda)=\frac{K_4(\lambda)}{K_5(\lambda)}-\lambda\frac{K_3(\lambda)}{K_5(\lambda)} \tag{A.2}$$

$$H(\lambda)=\frac{K_2(\lambda)}{K_5(\lambda)} \tag{A.3}$$

$$K^*(\lambda)=\lambda\frac{K_1(\lambda)}{K_5(\lambda)} \tag{A.4}$$

and

$$K_1(\lambda)=\frac{1}{252}\left[\frac{378}{5}N-46N^2+\frac{21}{2}M\left(\frac{11}{63}N-\frac{1}{5}\right)-\frac{M^2}{36}\right] \tag{A.5}$$

$$K_2(\lambda)=\frac{1}{252}\left[\frac{1}{18}M-\frac{21}{2}M\left(\frac{11}{63}N-\frac{1}{5}\right)\right]\frac{M}{\lambda} \tag{A.6}$$

$$K_3(\lambda)=\frac{2}{252}\left[\frac{378}{5}N-46N^2+\frac{21}{2}M\left(\frac{11}{63}N-\frac{1}{5}\right)-\frac{M^2}{36}\right]+\frac{1}{10}\left(3N-\frac{M}{12}\right) \tag{A.7}$$

$$K_4(\lambda)=2n+\frac{1}{6}M \tag{A.8}$$

$$K_5(\lambda)=\frac{1}{2}K_1(\lambda)-\lambda K_2(\lambda) \tag{A.9}$$

and,

$$N=1-\frac{1}{n} \tag{A.10}$$

$$M=\left(1-\frac{1}{n^2}\right)\lambda \tag{A.11}$$

$$\lambda=\frac{\delta^2}{v}\frac{\mathrm{d}U}{\mathrm{d}x} \tag{A.12}$$

$$Z=\frac{\delta^2}{v}\frac{U_\infty}{R} \tag{A.13}$$

By using a temperature distribution in the thermal boundary layer similar to the velocity distribution in the viscous boundary layer, we get:

$$\frac{T-T_0}{T_\infty-T_0}=2\left(\frac{y}{\delta_t}\right)-2\left(\frac{y}{\delta_t}\right)^3+\left(\frac{y}{\delta_t}\right)^4 \tag{A.14}$$

so that a differential equation for the ratio of the boundary layer thickness can be obtained

$$\frac{\mathrm{d}\xi}{\mathrm{d}\gamma}=\frac{1}{H_2(\lambda,\xi)}\left\{\frac{1}{\lambda Pr}\frac{\cos\gamma}{\sin\gamma}-H_1(\lambda,\xi)\xi\frac{\cos\gamma}{\sin\gamma}-\frac{1}{4}H_1(\lambda,\xi)\xi\frac{1}{Z}\frac{\mathrm{d}Z}{\mathrm{d}\gamma}-\frac{3}{2}H_3(\xi)\frac{\mathrm{d}Z}{\mathrm{d}\gamma}\cos\gamma+\frac{3}{2}H_3(\xi)Z\sin\gamma\right\} \tag{A.15}$$

$$H_1(\lambda,\xi)=\frac{3}{10}(1-N)\xi+\frac{1}{15}\left(2N+\frac{1}{6}M\right)\xi^2-\frac{1}{84}M\xi^3-\frac{1}{140}\left(3N-\frac{3}{4}M\right)\xi^4+\frac{1}{180}\left(N-\frac{1}{6}M\right)\xi^5 \tag{A.16}$$

$$H_2(\lambda,\xi)=\frac{3}{20}(1-N)\xi+\frac{1}{15}\left(2N+\frac{1}{6}M\right)\xi^2-\frac{1}{56}M\xi^3-\frac{3}{70}\left(N-\frac{1}{4}M\right)\xi^4+\frac{1}{72}\left(N-\frac{1}{6}M\right)\xi^5 \tag{A.17}$$

$$H_3(\xi)=\left(\frac{1}{180}\xi^3-\frac{1}{168}\xi^4+\frac{3}{1120}\xi^5-\frac{1}{2160}\xi^6\right)\frac{M}{\lambda} \tag{A.18}$$

The ratio of boundary layers thickness, ξ, was calculated by solving Eqs. (A.1) and (A.15) simultaneously. For the front stagnation point, $\gamma=0$, the equations reduce to:

$$K(\lambda_0) - K^*(\lambda_0) = 0 \tag{A.19}$$

and

$$H_1(\lambda_0, \xi_0)\lambda_0\xi_0 = \frac{1}{Pr} \tag{A.20}$$

References

[1] H. Kalman, Y.H. Mori, Experimental analysis of a single vapour bubble condensing in subcooled liquid, Chem. Eng. J. 85 (2002) 197–206.

[2] H.R. Jacobs, B.H. Major, The effect of noncondensible gases on bubble condensation in an immiscible liquid, J. Heat Transfer 104 (1982) 487–492.

[3] L.W. Florschuetz, B.T. Chao, On the mechanics of vapor bubble collapse, J. Heat Transfer 87 (1965) 209–220.

[4] D.D. Wittke, B.T. Chao, Collapse of vapor bubbles with translatory motion, J. Heat Transfer 89 (1967) 17–24.

[5] S. Kamei, M. Hirata, Study on condensation of a single vapor bubble into subcooled water, part 2—experimental analysis, Heat Transfer—Japanese Res. 19 (1990) 1–10.

[6] M.O. Isikan, Condensation of spherical-cap shaped bubbles, Int. J. Heat Mass Transfer 33 (1990) 1099–1103.

[7] Y.M. Chen, F. Mayinger, Measurement of heat transfer and the phase interface of condensing bubbles, Int. J. Multiphase Flow 18 (1992) 877–890.

[8] O. Zeitoun, M. Shoukri, V. Chatoorgoon, Interfacial heat transfer between stream bubbles and subcooled water in vertical upward flow, Trans. ASME, J. Heat Transfer 117 (1995) 402–407.

[9] H.R. Jacobs, H. Fannar, G.C. Beggs, Collapse of a bubble of vapor in immiscible liquid, in: Proceedings of the Sixth International Heat Transfer Conference, vol. 2, 1978, pp. 383–388.

[10] J. Isenberg, D. Moalem, S. Sideman, Direct contact heat transfer with change of phase: bubble collapse with translatory motion in single and two-phase systems, in: Proceedings of the Fourth International Heat Transfer Conference, vol. 5, 1970, p. B.2.5.

[11] J. Isenberg, S. Sideman, Direct contact heat transfer with change of phase: bubble condensation in immiscible liquids, Int. J. Heat Mass Transfer 13 (1970) 997–1011.

[12] K. Higeta, Y.H. Mori, K. Komotori, Condensation of a single vapor rising in another immiscible liquid, AIChE Symp. Ser. 75 (189) (1979) 256–265.

[13] K. Higeta, Y.H. Mori, K. Komotori, A novel direct-contact condensation pattern of vapour bubbles in an immiscible liquid, Canadian J. Chem. Eng. 61 (1983) 807–810.

[14] H. Kalman, A. Ullmann, R. Letan, Dynamics of a condensing bubble in zones of time dependent velocity, in: Proceedings of the Eighth International Heat Transfer Conference, vol. 4, 1986, pp. 1925–1930.

[15] H. Kalman, A. Ullmann, R. Letan, Visualization studies of a freon-113 bubble condensing in water, J. Heat Transfer 109 (1987) 543–545.

[16] Y. Lerner, H. Kalman, R. Letan, Condensation of an accelerating–decelerating bubble: experimental and phenomenological analysis, J. Heat Transfer 109 (1987) 509–517.

[17] H. Kalman, R. Letan, Condensation of a bubble in an immiscible liquid: characteristics of the thermal resistance, in: Proceedings of the Heat Transfer Conference Symposium Series 257, vol. 83, 1987, pp. 128–133.

[18] H. Kalman, A. Ullmann, Experimental analysis of bubble shape during condensation in miscible and immiscible liquids, J. Fluids Eng. 121 (1999) 496–502.

[19] Y. Lerner, Condensation of bubbles, M.Sc. Thesis, Ben-Gurion University of the Negev, Beer Sheva, Israel, 1983.

[20] A. Ullmann, R. Letan, Effect of noncondensibles on condensation and evaporation of bubbles, Trans. ASME, J. Heat Transfer 111 (1989) 1060–1067.

[21] Y. Lerner, R. Letan, Dynamics of condensing bubbles: effects of injection frequency, ASME paper no. 85-HT-47, 1985.

[22] K. Lee, H. Barrow, Transport processes in flow around a sphere with particular reference to the transfer of mass, Int. J. Heat Mass Transfer 11 (1968) 1013–1026.

[23] H. Schlichting, Boundary Layer Theory, McGraw-Hill, New York, 1979.

[24] H. Kalman, R. Letan, Thickness of thermal and velocity boundary layers on a mobile surface of a sphere, Int. Commun. Heat Transfer 12 (1985) 201–208.

[25] S. Tomotika, The laminar boundary layer on the surface of a sphere in a uniform stream, Brit. Aero. Res. Com. R.M. No. 1678, 1935, pp. 86–98.